CrossMark

Hysteresis in magnetoresistance and formation of spin glass like structure in PVA capped Fe_3O_4

Surajit Ghosh[1] · Prayas Chandra Patel[1] · P. C. Srivastava[1]

Abstract Here, we report the temperature dependent hysteresis in the magneto transport in PVA capped Fe_3O_4 nanoparticles. The synthesis of the nanoparticles of size 10–15 nm were carried out via co-precipitation method followed by heat treatment at different temperatures. Structural studies confirm the formation of polycrystalline Fd $\bar{3}m$ phase of Fe_3O_4 when the samples were sintered up to 600 °C. FTIR studies show that PVA and magnetic grains were attached through hydrogen bonding between hydroxyl group of PVA and protonated surface of the oxide. Spin glass type transition was observed in the ZFC–FC plots at 125 K which is also the Verwey transition temperature T_V as measured from the transport studies. A hysteresis in the MR plot was found which was explained in the realm of tunnel transport through ferromagnetic grain and anti-ferromagnetic surface of the ferrite particles. Tunnelling through the dielectric spacer layer of PVA has an overall impact to increase the resistance of the samples. The temperature dependence of the hysteresis gives a major hint to the origin of the spin glass type behaviour of the samples.

1 Introduction

The experimental observation of Verwey transition in the nano form of magnetite, a hallmark in the study of magnetite (Fe_3O_4), has stimulated unprecedented research activities in the field of nanomagnetism in the ferrite material [1–9]. In Verwey transition, the system undergoes a metal–insulator first order phase transition on lowering the temperature below 120 K [10]. The dependence of the transition temperature on various factors like particle size, stoichiometry, substrate induced stress in thin films, presence of anti-phase boundaries (APB) and oxygen vacancies etc. has evoked many questions regarding the mechanism of the transition in nanostructures of Fe_3O_4 [1–3, 5]. A significant change in magnetoresistance (%MR) in different Fe_3O_4 nanoparticles and thin films near T_V has also been a matter of great interest [6, 9, 11]. Fe_3O_4 is a well known ferrimagnetic material at room temperature (RT) owing to its inverse spinel structure in which there are two types of sites; tetrahedral (A) and octahedral (B) in the face centred cubic lattice of oxygen. 'A' sites are fully occupied by Fe^{3+} ions while 'B' sites are equally shared among Fe^{3+} and Fe^{2+}. The magnetic moments of the A and B sites are aligned in antiparallel orientation to each other, resulting in the cancellation of the moment of Fe^{3+}, thus forming a collinear ferrimagnetic ordering with Curie temperature ~860 K [12]. Continuous hopping of electrons between Fe^{2+} and Fe^{3+} is responsible for the material being a good conductor at RT. It is assumed that the electrons get localised below T_V so that the hopping stops, thus by making the material insulator [13]. The magnetic behaviour of the system when it undergoes Verwey transition is still a matter of debate [14, 15]. Although there are several reports on Fe_3O_4 nanoparticles behaving as a spin glass system at low temperature, the true origin of their spin glass type behaviour is still under the scanner [16, 17].

Synthesis of Fe_3O_4 nanoparticles has been an activity of interest for a long time because of its immense technological applications pertaining to its several exciting properties such as good conductivity, half metallic nature, high Curie temperature etc. [18]. Several techniques have been

✉ P. C. Srivastava
pcsrivastava50@gmail.com

1 Solid State Electronics and Magneto-Electronics Laboratory, Department of Physics, Institute of Science, Banaras Hindu University, Varanasi, U.P. 221005, India

employed to synthesize Fe_3O_4 nanoparticles; the challenge being to control the particle size as the particles tend to agglomerate very easily in case of ferrite materials. The difficulty in controlling the particle size along with the oxidising nature of Fe_3O_4 (even at 150 °C) can be sorted out by capping/coating the magnetic nanoparticles with different materials, such as, polymers, TiO_2, SiO_2 etc. [19]. Polyvinyl alcohol (PVA), a common hydrophilic and biocompatible coating material which is diamagnetic and dielectric in nature, prevents agglomeration of nanoparticles resulting in the formation of monodispersed particles [20, 21]. Additionally, the multi-hydroxyl structure of PVA enhances crystallinity of the synthesized particles, resulting in desirable thermo-mechanical properties such as high elastic modulus, crystallinity and tensile strength etc. [21, 22].

In this context, we report here a successful synthesis (via co-precipitation method) of PVA capped Fe_3O_4 nanoparticles, followed by thermal treatment at different temperatures to have different particle size. The impact of particle size on many of its structural, transport and magnetic properties were investigated through different measurements. The structural evolution of thermally treated particles in terms of phases and their dimension were studied through XRD, SEM, TEM and FTIR measurements. Another aspect of the synthesized magnetic nanoparticles being spin glass particles below T_V was investigated through temperature dependent transport and magnetic measurements. Interestingly, hysteresis was observed in the MR plot which was found to be temperature dependent. These observations were understood in the realm of formation and tunnelling of charge carriers through surface spin clusters that behave as a spin glass system. The role of dielectric spacer layer separating ferromagnetic grains has also been invoked.

2 Experimental details

The polyvinyl alcohol (PVA) coated Fe_3O_4 nanoparticles were synthesized via co-precipitation method [23] using $FeCl_2 \cdot 6H_2O$ and $Fe(NO_3)_3 \cdot 9H_2O$ as the precursors of Fe^{2+} and Fe^{3+} ions respectively with double distilled water as the solvent. An aqueous solution of the polymer was made by dissolving it in 100 ml deionised water at 250 °C. A 250 ml solution of 0.04 M $FeCl_2 \cdot 6H_2O$ and 0.08 M $Fe(NO_3)_3 \cdot 9H_2O$ was prepared to keep Fe^{2+} and Fe^{3+} ions in proper stoichiometric ratio (1:2). 35.1 ml of 30% ammonia solution was added drop wise to the solution under vigorous stirring (600 rpm). Then, the polymer solution was added to it with continuous stirring which was kept for 3 h at room temperature to get a homogeneous mixture. The black precipitate so formed was filtered out and rinsed with distilled water several times to remove impurities and was dried in an electrical oven at 80 °C. The dried samples were grinded in

an agate mortar to obtain the powder samples which were sintered at 400, 500, 600 and 700 °C at 10^{-3} Torr for 6 h. The samples were allowed to cool down naturally and were taken for further analysis. The samples sintered at 400, 500, 600 and 700 °C were named as FO_400, FO_500, FO_600 and FO_700 respectively. The synthesis route i.e., addition of polymer solution at the final stage to get the capped or coated magnetic nanoparticles have also been employed by several other researchers [24].

Structural analysis of the powder samples was done using the X-ray (XRD) diffractograms obtained from "X'Pert Pro PANalytical" diffractometer (CuK$_\alpha$ $\lambda = 1.54060$ Å). "QUANTA 200 F" scanning electron microscope (SEM) and FEI: Tecnai 20G^2 transmission electron microscopes (TEM) were used for the microstructure investigation. Fourier transform infrared spectroscopy (FTIR) measurements were done by Shimadzu "IR-Affinity1 spectrophotometer". Magnetic properties of the samples M–H (at room temperature) and M–T were recorded using Microsense EV9 vibrating sample magnetometer (VSM) and SQUID magnetometer from Quantum Design respectively. The resistivity measurements were carried out by the linear four probe method using physical property measurement system (PPMS-QD, 2 K/14 T).

3 Result and discussion

3.1 Structural and morphological analysis

Figure 1 shows the X-ray diffraction patterns of PVA coated Fe_3O_4 nanoparticles (FO_400, FO_500, FO_600 and FO_700) in the 2θ range of 15°–80°. FO_400, FO_500 and FO_600 show similar diffraction patterns and
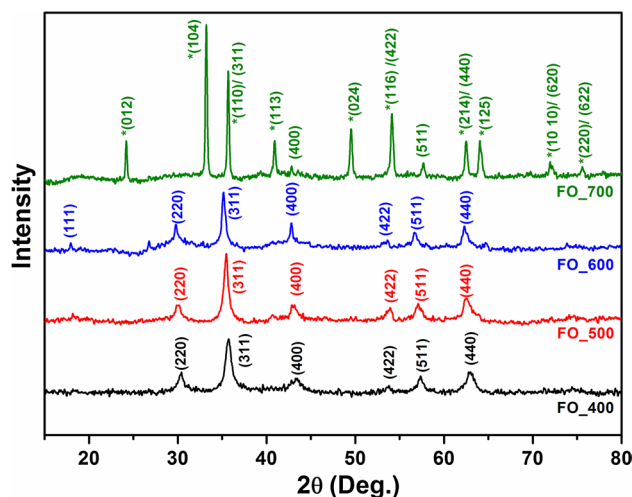

Fig. 1 XRD patterns of Fe_3O_4 nanoparticles sintered at different temperature

correspond to Fe_3O_4 whereas the peaks of FO_700 match with those of α-Fe_2O_3 phase. The diffraction patterns of FO_400, FO_500, and FO_600 match well with the standard JCPDS card no. 653107 and the peaks at $2\theta = 18.23$, 29.97, 35.39, 36.96, 43.01, 53.58, 57.07 and 62.70 were indexed to the reflection planes 111, 220, 311, 222, 400, 422, 511 and 440 respectively. Since no other impurity peak corresponding to any secondary phase/compound could be detected, the formation of pure single phase Fe_3O_4 with a face centred cubic structure with the space group Fd $\bar{3}m$ can be ascertained for these three samples. The diffraction peaks of FO_700 match with standard JCPDS data of α-Fe_2O_3 (card no. 890599). Few low intensity peaks of FO_700 (Fig. 1), instead of matching with Fe_2O_3 match with Fe_3O_4 while few others can be indexed to both Fe_2O_3 and Fe_3O_4. It shows that the material converts itself from Fe_3O_4 to Fe_2O_3 on sintering above 600 °C, though the complete conversion may not occur at 700 °C and traces of Fe_3O_4 could still be detected. With the increase of sintering temperature, intensity of the diffraction peaks increases while full width at half maxima (FWHM) decreases, resulting in gradual sharpening of the peaks which obviously indicates enhancement in the crystalline nature of the nanoparticles. The average particle size was determined from the full width at half maxima (FWHM) using the well known Debye–Scherrer relation and were found to be ~10, 13 and 15 nm for FO_400, FO_500 and FO_600 respectively. Thus, the average particle size was found increasing slightly with the sintering temperature.

The surface morphological features of the Fe_3O_4 nanoparticles as observed from the SEM micrograph are shown in Fig. 2 at a magnification of 10 μm. Structures of random shape and size, agglomerated in small clusters of size ranging from 1 to 5 μm are distributed homogeneously throughout the samples. The agglomeration can be understood by the high surface energy as a result of higher surface to volume ratio for smaller particles. A secondary grain growth can also be seen in the SEM images which can also be the result of high surface energy.

Figure 3a, b show the TEM image of FO_400 and FO_600 and show the formation of polycrystalline nanoparticles with average size of ~10 and ~15 nm respectively which are consistent with the XRD results. The results also indicate that the particles sintered at 400 and 600 °C are uniform in morphology over the entire scan area. It is very difficult to control the size of Fe_3O_4 nanoparticles as they tend to agglomerate very easily into larger grains due to their higher surface energy. The coating/capping of the
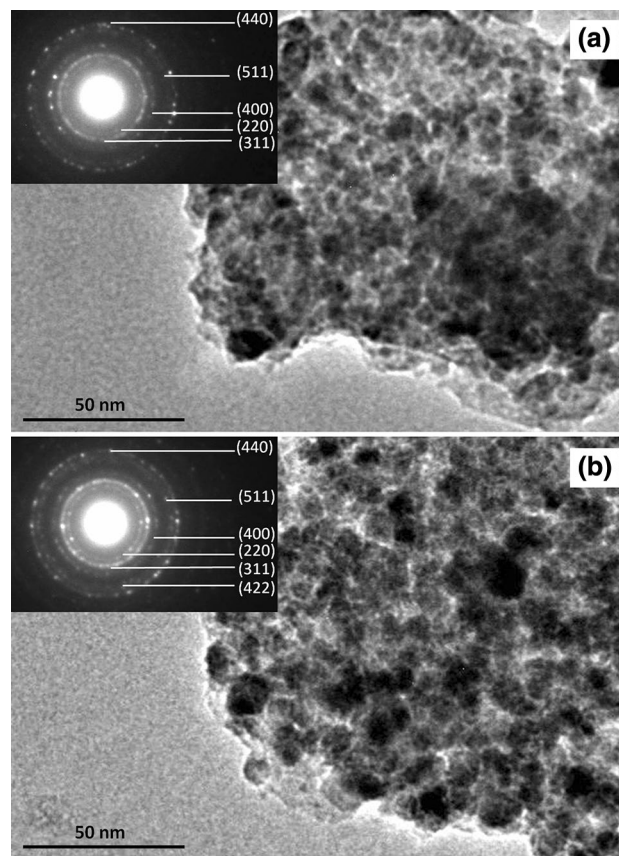

Fig. 3 TEM images of **a** FO_400 and **b** FO_600. *Inset* shows corresponding SAED patterns
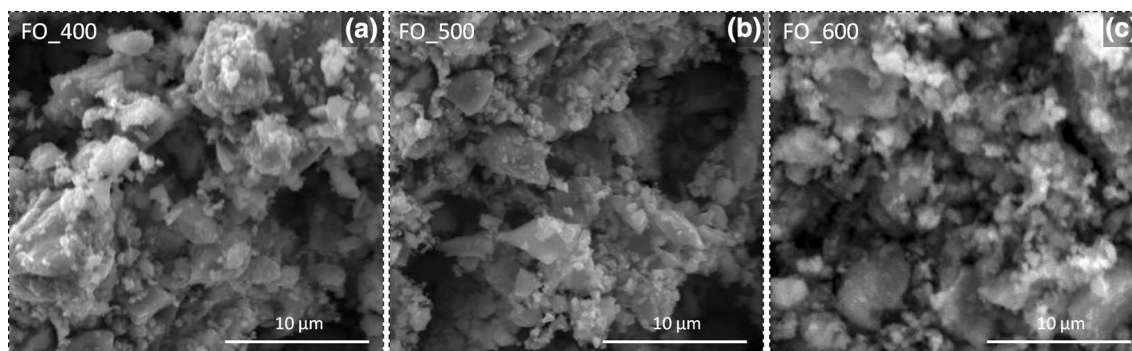

Fig. 2 SEM micrographs of PVA capped Fe_3O_4 nanoparticles

nanoparticles by the polymer does the trick here to restrict them from agglomerating thus producing nanoparticles with nearly uniform shape and size. The rings observed in the selected area electron diffraction pattern (SAED) (insets) confirm the polycrystalline nature of the samples with lattice parameter consistent with fcc phase in Fd $\bar{3}m$ space group of Fe_3O_4, revealing no perceivable lattice distortion. The diffraction planes corresponding to the rings are consistent with the planes observed in XRD.

Thus, from the structural analysis it can be concluded that the spinel structured Fe_3O_4 nanoparticle are formed up to the sintering temperature of 600 °C, after which it oxidises to become Fe_2O_3 at 700 °C. Since uncoated Fe_3O_4 can oxidise even at a very tender temperature of 150 °C, it is difficult to sinter it at higher temperature to get crystalline nanoparticles. But in our case by using PVA as a coating/capping agent we could sinter the samples up to 600 °C without getting them oxidised and get better crystalline particles. It is also very difficult to restrict the magnetic spinel ferrite particles from agglomerating, which was also made possible via coating of the nanoparticles with the polymer.

3.2 FTIR study

FTIR is a very significant tool for finding the attachment of polymer to the magnetic nanoparticles as well as for finding the correlation between conjugant atoms of the magnetic nanoparticles. Fe_3O_4 crystallises into inverse spinel structure in which there are tetrahedral A sites (8A) occupied by half of the Fe^{3+} cations and octahedral B sites (16B) occupied by Fe^{2+} ions and the rest of the Fe^{3+} ions. Out of the 13 normal modes predicted from the factor group analysis [25] for the inverse spinel structure, two are IR active ($2T_{1U}$), which can be seen in the FT-IR spectra (Fig. 4) measured in the range 400–4000 cm^{-1}. The bands at ~620 and 440 cm^{-1} observed for FO_400, FO_500 and FO_600 are the signature bands of Fe_3O_4 phase corresponding to metal–oxygen bonds i.e., υ vibrations of Fe_{TH}–O–Fe_{OH} and Fe_{OH}–O stretching mode respectively [19, 26]. Fe_{TH} and Fe_{OH} refer to the Fe ions occupying the tetrahedral and octahedral positions. Little improvement in the intensity of these bands with the sintering temperature could be seen in context to the small enhancement in the crystallinity of the Fe_3O_4 nanoparticles. Further, shifts in the bands ~620 and ~440 cm^{-1} are observed in spectrum of FO_700 which is obvious as the nanoparticles got oxidised to Fe_2O_3 (also seen from the XRD results). The broad bands at 3200 and 1630 cm^{-1} are attributed to the stretching modes of O–H group and H–O–H bending vibration which show the presence of absorbed/adsorbed water [27]. The band at ~1400 cm^{-1} could be due to the anti-symmetric NO_3^- stretching vibration that arises from the residual nitrate groups [27] of the $Fe(NO_3)_3$ used as the
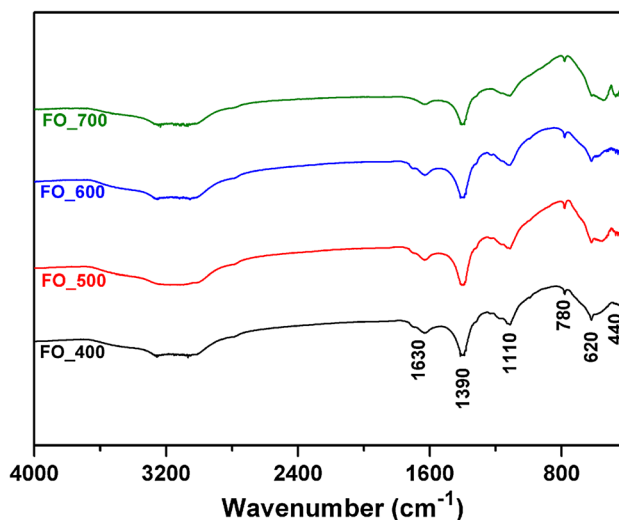

Fig. 4 FTIR spectra of PVA capped Fe_3O_4 nanoparticles sintered at different temperature

precursor as well as to the C–C vibrations arising from the polymer chain [19]. Since the intensity of the peak does not decrease with the sintering temperature, we could conclude it to be due to the C–C vibrations as at such high temperatures like 700 °C, NO_3 would decompose. The most important feature of the FTIR spectra can be observed in the band at 1110 cm^{-1} which attributes to the Fe–O–C bond and is due to the attachment of PVA to the magnetic Fe_3O_4 nanoparticles. The bands at ~3020 and 790 cm^{-1} are assigned to the C–H vibrations and CH_2 rocking mode respectively [19]. Similar interaction of polymer PVA with the magnetic Fe_3O_4 particles has earlier been investigated by Kayal et al. [19] to find that the attachment of PVA to Fe_3O_4 occurs via hydrogen bonding between hydroxyl group of PVA and protonated surface of the oxide.

It can be concluded that the synthesized sample retains its spinel structure of Fe_3O_4 phase with a little improvement of its crystalline behaviour up to the sintering temperature 600 °C beyond which it gets oxidised to Fe_2O_3. It is also found that the polymer PVA is attached to Fe_3O_4 through hydrogen bonding in all the samples, sintered even at higher temperatures.

3.3 Magnetic characterization

To study the magnetic properties of the synthesized samples the temperature dependence of magnetization, Zero-field-cooled (ZFC) and field-cooled (FC) magnetization were measured with an applied low field of 100 Oe for FO_400 FO_500 and FO_600. The ZFC–FC magnetization curves were recorded by cooling the samples to 10 K in presence of zero magnetic field H = 0 (ZFC) and H = 100 Oe (FC) and recording the magnetization on

raising the temperature up to 300 K in H = 100 Oe. The blocking temperature (T_b) of the system must be above room temperature since the ZFC–FC curves are well apart even at 300 K, as shown in Fig. 5. The diverging nature of the ZFC and FC curves below 300 K in all the samples indicates that the nanoparticles are strongly coupled by exchange interactions in our system [28]. With increase of sintering temperature the separation between ZFC and FC curves decreases which means the interactions between particles become weaker. For all the samples the FC magnetization shows a tendency to saturate at low temperature region. The value of maximum FC magnetization decreases for the samples sintered at higher temperature, which indicates that the rise in sintering temperature increases magnetic anisotropy. The increase in magnetic anisotropy could be understood to be due to enhancement in the crystallinity of the samples with higher sintering temperature as observed from the structural study. It also indicates that the sintering temperature enhances the ferrimagnetic moment which can be due to the decrease in the exchange interaction [28, 29].

The sample FO_600 shows a kink in the FC curve at 125 K. For the ZFC curve, a sharp decrease in magnetization below 125 K is observed, while for FC the magnetization remains almost constant with decrease in temperature. The anomalous trend in variation of magnetization with temperature could be related either to the spin reorientation transition (or spin glass transition) or to the modification introduced as a result of Verwey transition or both. Such type of behaviour in FC or ZFC curves has earlier been reported for Fe_3O_4 and was attributed to changes in the magnetic order due to Verwey transition [11, 18]. Gaikward and Acharya [30] have reported similar thermo-magnetization behaviour for $BiFeO_3$ nanoparticles as result of spin glass transition.

The spin glass state generally occurs when positions of magnetic moments or sign of neighbour coupling appear in random manner. This combination of magnetic randomness and mixed interaction causes frustration and stochastic disorder in the corresponding energy landscape [31]. The physics of Verwey transition which is nearly 75 years old is still not very clear. The Verwey transition as explained by Verwey is based on charge ordering model. It seems that the charge ordering is also related with their spin ordering as we could observe a transition similar to spin glass transition near Verwey transition. As the system undergoes the transition temperature, the localisation of Fe^{3+} ions, the spins of which are antiparallel to that of Fe^{2+} ions (above the transition temperature), is believe to happen to reorient the spins of the system. As a result, the ZFC magnetization decreases abruptly below the transition temperature. It is important to note that several factors such as spin frustration at the surface of individual nanoparticles, inter-particle interactions etc. give rise to the SG like behaviour [16, 31, 32]. There are several reports available on whether Fe_3O_4 behaves as a true spin glass system or is it the FM–AFM interaction between the ferrite particles that is causing the memory effect in the system [16, 17, 33]. Suzuki et al. [17], showed the existence of super spin glass behaviour in their chemically synthesized Fe_3O_4 nanoparticles from the memory effect observed in ZFC–FC protocol. Yang et al. [33], showed that the SiO_2 mediated inter-particle spacing effectively modulates the collective behaviour of Fe_3O_4 nanoparticles. Gandhi et al. [16], have shown from their ZFC magnetization study that memory effect in their pseudo-spherical Fe_3O_4 nanoparticle came from the weak inter-particle interaction among the ferrite particles. So, at this point it is very hard to comment on the origin of spin glass type behaviour of the samples.

For FO_600, Verwey transition can be clearly seen in the low temperature resistivity measurement (shown in the inset of Fig. 5c), where the resistivity of the system changes abruptly by almost three orders at ~125 K. Thus, in our case the Verwey transition temperature measured from both the resistivity plot and the ZFC–FC magnetization curves are same. Moreover, the overall resistivity of the
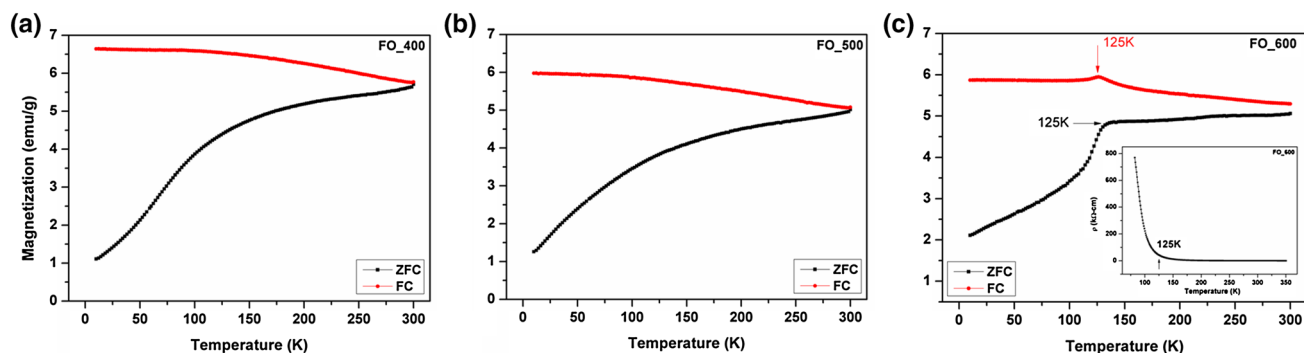

Fig. 5 Temperature dependence of magnetization with ZFC–FC process of **a** FO_400, **b** FO_500 and **c** FO_600 measured at an applied field of 100 Oe. *Inset* in the **c** shows the resistivity vs temperature plot of FO_600

sample was very large compare to that of bulk or uncoated nanoparticles. It is obvious as the coating of PVA, a well known insulator, must have played important role as spacer layer between the ferromagnetic grains in inter-granular tunnelling in the sample, making the transport more difficult. Interestingly, for FO_400 and FO_500 no such kink or sharp transition could be observed, though gradual decrease in the ZFC magnetization was observed. The saturation of FC magnetization in both the samples at low temperature suggests their spin glass type behaviour at low temperatures. The transition depends upon many factors, such as, nanosize effect, induced strain, lattice disorder and applied magnetic field etc [30, 34, 35]. The particle sizes of these two samples were smaller than that of FO_600 which could have played a dominating role in disappearing sharp transition in those samples. Moreover, we also could not record the resistivity data for those two samples also as the resistivity of the samples were too high to measure via four-probe method. The dielectric spacer layer of PVA might have also affected the conductivity of these samples.

Further, magnetization study of the samples FO_400, FO_500 and FO_600 from M–H hysteresis loop (Fig. 6) shows ferromagnetic behaviour at room temperature. The values of coercivity (H_C) and saturation magnetization (M_S) of the samples from the hysteresis loop were found lower in comparison to bulk Fe_3O_4. It is evident that the magnetic interaction gets stronger with the increase of sintering temperature as the saturation magnetization were found to increase with higher sintering temperature.

The saturation magnetization of FO_600 (92 emu) nearly approaches the value of bulk Fe_3O_4 (115 emu g^{-1}) [18]. Inset (a) of Fig. 6 shows the expanded view of hysteresis loop around origin (from −200 to 200 Oe). The variations of M_S and H_C as a function of sintering temperature are shown in the inset of Fig. 6, which shows both H_C and M_S increases almost linearly with sintering temperature. The magnetic behaviour of typical soft ferromagnetic materials like Fe_3O_4 is believed to be significantly influenced by the synthesis route and particle size. In very small magnetic nanoparticles the surface spin disorder plays an important role in determining the saturation magnetization, causing it to be much lower than bulk value [36–38]. Therefore, the enhanced saturation magnetization for the samples with higher sintering temperature can be understood on the basis of domain structure, critical size, magnetic anisotropy, cation redistribution, surface spin and formation of spin glass structures [39–42]. Moreover, for relatively larger particles the static magnetic energy gets reduced because of formation of larger magnetic domains in such particles. The average particle sizes of our samples were found out to be ~10–16 nm. Thus, these particles can form single domain structure whose magnetic behaviour can be explained on the basis of the well known Stoner–Wohlfarth model [43]. According to the model, as the particle size increases, the coercivity of the "single-domain" particle assembly increases progressively, since the magnetic moment of the individual particle increases and the magnetic anisotropy energy

Fig. 6 M–H characteristics of pva Capped Fe_3O_4 nanoparticles measured at room temperature. *Inset* shows (*a*) expanded view of hysteresis loop and (*b*) variation of H_C and M_S with sintering temperature
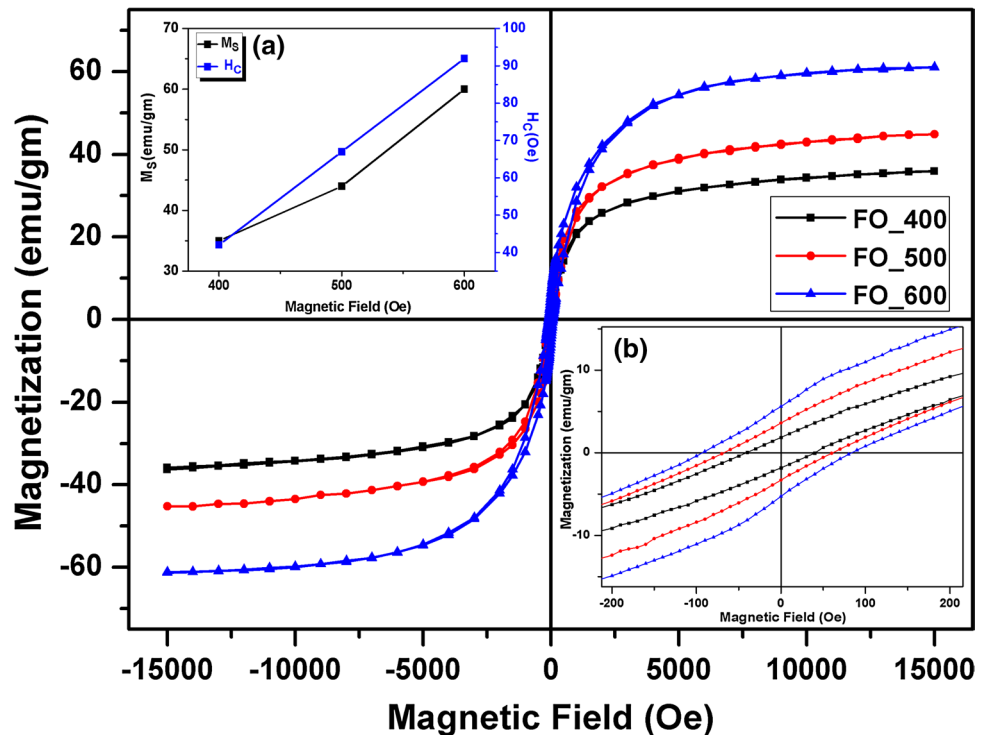
increases. Thus, the increase of coercive field with increase of particle size can be understood by the model.

Thus, from ZFC–FC and M–H characteristics, it is observed that the nanostructure system undergoes a spin glass like transition on lowering the temperature below 125 K, at which the system also undergoes Verwey transition. It seems that both these transitions are not separate but interconnected, i.e., the system undergoes a transition or structural modification whose effect can be seen in both magnetic properties and electrical properties separately in ZFC–FC and resistivity measurements. The transition was found dependent on the particle sizes and the dielectric spacer layer of PVA, as the samples with particle size less than a certain limit do not show sharp spin glass like transition and high conductivity.

3.4 Magneto-transport study

Figure 7a–e shows the dependence of magnetoresistance (%MR) with magnetic field of the sample FO_600 at different temperatures. The %MR was calculated using the formula $\%MR = \frac{\rho(H) - \rho(0)}{\rho(0)} \times 100$, where $\rho(H)$ and $\rho(0)$ are the resistivity of the sample with and without applied magnetic field. The sample shows a negative MR which increases with magnetic field at all the temperatures with maxima at highest applied field of 12 T. Fig. 7f shows variation of maximum %MR with the temperature showing a peak at 125 K which is the Verwey transition temperature of the sample. The value of MR maxima increases while decreasing the temperature until the Verwey transition

temperature. After that the system becomes insulating and below 100 K, the resistivity becomes so high that it was not possible to measure the resistivity via four probe method. The occurrence of maximum MR at Verwey transition has earlier been reported [7, 11] and were attributed to the sudden change in the magnetic order of the system due to Verwey transition. The changes in the magnetic order have clearly been seen for our sample. The most interesting part of the result is that the MR variation shows hysteresis which goes on decreasing as the temperature is lowered. The maximum hysteresis was observed at 250 K which goes on decreasing to 125 K where the sample shows almost negligible hysteresis. The behaviour of the hysteretic dependences of the magnetoresistance implies that the sample remembers its magnetic state determined by the applied field. The magnetoresistance of the system is sensitive to its magnetic state. The hysteresis in the magnetoresistance has been reported earlier in different rare earth manganites [44, 45]. The low temperature behaviour of the electrical resistance in those cases was explained either by spin dependent tunnelling of charge carriers via dielectric spacers separating ferromagnetic grains [44] or by formation of a network of ferromagnet–antiferromagnet–ferromagnet tunnel contacts [45]. Though, the temperature dependence of hysteresis in the magnetoresistance has not been reported earlier. In our sample also there is a dielectric spacer layer made of PVA which might have influenced the spin dependent tunnelling of the charge carriers between ferromagnetic grains of Fe_3O_4. The decrease of hysteresis indicates that the dependence of spin state of the charge carriers in inter-granular tunnelling is temperature
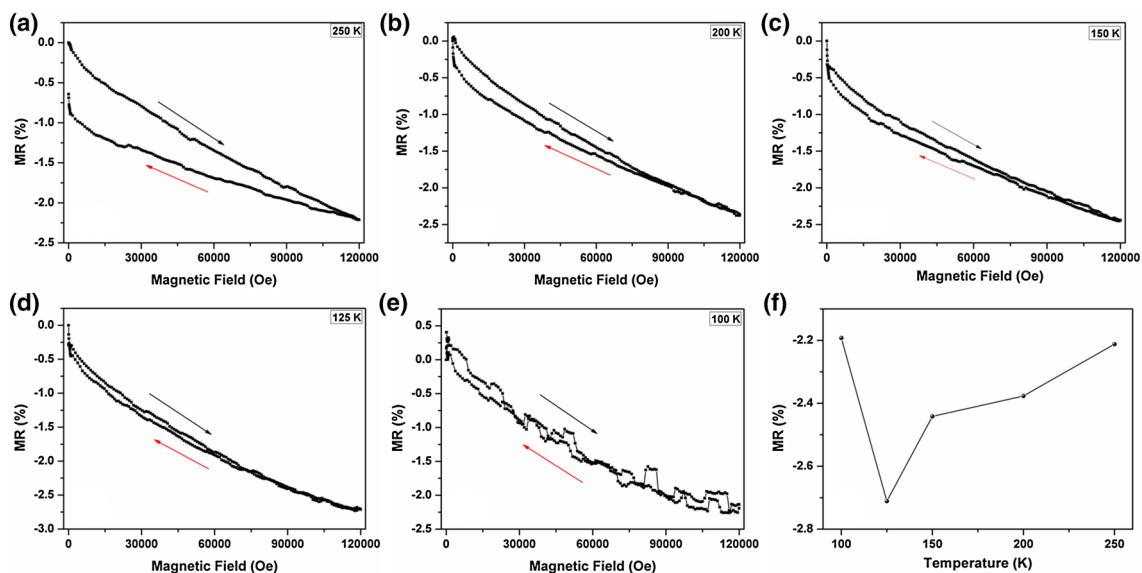

Fig. 7 %MR versus applied magnetic field plot of FO_600 at **a** 250 K, **b** 200 K, **c** 150 K, **d** 125 K and **e** 100 K. **f** Shows the variation of maximum %MR with temperature

dependent. This dependence can be understood by considering a grain–surface model consisting of ferromagnetic grain and antiferromagnetic surface separated by anti-phase boundary (APB). The formation of APB is very common in case of Fe_3O_4 nanoparticles [6]. The application of magnetic field makes the surface spins pinned according to the near surface spins of the ferromagnetic grains, reducing the resistance of the system as the ordered system faces less spin scattering. Now, when magnetic field is lifted off, the surface spins remain pinned to the near surface spins of the grains, so that the magnetoresistance plot shows a hysteresis. Tunnelling of the electrons via the AFM layer and the dielectric spacer layer of PVA thus play a pivotal role in determining the magnetoresistance of the system. When the temperature is decreased, the surface spin fluctuations become weaker so that a short range ordering between surface spin develop. This could result in a progressive formation of magnetically correlated spin regions of growing size and finally giving rise to a frozen disordered surface-spin state that could resemble a cluster of spin glass state [46, 47]. Thus at low temperature, the decrease of the hysteresis area in the MR curve can be explained as this cluster or disordered states eventually diminish the possibility of pinning of spins at the surface. Thus, the ambiguity over the origin of the spin glass like behaviour of the system at low temperature (observed in ZFC–FC measurement) can now be understood to be due to the FM–AFM interaction between the ferrite particles.

4 Conclusion

PVA capped Fe_3O_4 nanoparticles were successfully synthesized via co-precipitation method followed by sintering at different temperatures. Spinel Fe_3O_4 particles of 10–15 nm with phase group Fd $\bar{3}m$ were found from the XRD pattern. Particles of samples with higher sintering temperature were also found to be of better crystallinity, with SAED pattern showing polycrystalline nature of the samples. FTIR spectra confirmed the spinel structure of the ferrite and the attachment of PVA to the magnetic grains through hydrogen bonding. The blocking temperature of the samples was estimated to be above room temperature. For the sample FO_600 spin glass type behaviour were observed in the ZFC–FC measurement with spin glass type transition at 125 K. From the resistivity measurement the Verwey transition was observed for the sample FO_600 at 125 K. It seems that the well known charge ordering theory of Verwey transition is linked with its magnetic ordering also. The ferromagnetic properties, significantly influenced by the structural changes due to the heat treatment and resulting in the increase of M_S and H_C values were understood in terms

of Stoner–Wohlferth model. Interestingly an uncommon feature of hysteresis was observed in the MR vs applied field plot at different temperature which was explained considering spin dependent tunnel transport across ferromagnetic gain and antiferromagnetic surface. The surface spin fluctuations being weak at low temperature, the hysteresis gets diminished at low temperature. Thus, the origin of the spin glass type behaviour of the sample was understood in the realm of ferromagnetic–antiferromagnetic interaction among the ferrite particles.

References

1. J.P. Shepherd, J.W. Koenitzer, R. Aragon, J. Spalek, J.M. Honig, Heat capacity and entropy of nonstoichiometric magnetite $Fe_{3(1-\delta)}O_4$: the thermodynamic nature of the Verwey transition. Phys. Rev. B **43**, 8461–8471 (1991)
2. D.T. Margulies, F.T. Parker, F.E. Spada, R.S. Goldman, J. Li, R. Sinclair, A.E. Berkowitz, Anomalous moment and anisotropy behavior in Fe_3O_4 films. Phys. Rev. B **53**, 9175–9187 (1996)
3. P. Novák, H. Štêpánková, J. Englich, J. Kohout, VAM Brabers, NMR in magnetite below and around the Verwey transition. Phys. Rev. B **61**, 1256–1260 (2000)
4. J. Tang, K.Y. Wang, W. Zhou, Magnetic properties of nanocrystalline Fe_3O_4 films. J. Appl. Phys. **89**, 7690–7692 (2001)
5. P. Poddar, T. Fried, G. Markovich, First-order metal-insulator transition and spin-polarized tunneling in Fe_3O_4 nanocrystals. Phys. Rev. B **65**, 172405 (2002)
6. D. Tripathy, A.O. Adeyeye, S. Shannigrahi, Magnetic and tunneling magnetoresistive properties of an all-oxide Fe_3O_4–Al_2O_3 granular system. Phys. Rev. B **76**, 174429 (2007)
7. X. Wang, Y. Sui, J. Tang, C. Wang, X. Zhang, Z. Lu, W. Su, X. Wei, R. Yu, Amplification of magnetoresistance of magnetite in an Fe_3O_4–SiO_2–Si structure. Appl. Phys. Lett. **92**, 012122 (2008)
8. H. Yan, M. Zhang, H. Yan, Electrical transport, magnetic properties of the half-metallic Fe_3O_4-based Schottky diode. J. Magn. Magn. Mater. **321**, 2340–2344 (2009)
9. S. Ghosh, N. Srivastava, P.C. Srivastava, Injecting electrode controlled electronic transport across Fe_3O_4 film-Si interfacial structure. J. Alloy. Compd. **612**, 418–424 (2014)
10. E.J.W. Verwey, Electronic conduction of magnetite (Fe_3O_4) and its transition point at low temperatures, Nature **144**, 327–328 (1939)
11. T.L. Qu, Y.G. Zhao, H.F. Tian, C.M. Xiong, S.M. Guo, J.Q. Li, Rectifying property and giant positive magnetoresistance of Fe_3O_4/SiO_2/Si heterojunction. Appl. Phys. Lett. **90**, 223514 (2007)
12. C. Kittel, *Introduction to Solid State Physics*, 8th edn. (Wiley, New York, 2004)
13. E.W.J. Verwey, P.W. Haaymann, F.C. Romeijn, Physical properties and cation arrangement of oxides with spinel structures II. Electronic conductivity. J. Chem. Phys. **15**, 181–187 (1947)
14. F. Walz, The Verwey transition—a topical review. J. Phys. **14**, R285–R340 (2002)
15. J. García, G. Subías, The Verwey transition—a new perspective. J. Phys. **16**, R145–R178 (2004)

16. A.C. Gandhi, P.M. Reddy, T.S. Chan, Y.P. Ho, S.Y. Wu, Memory effect in weakly-interacting Fe_3O_4 nanoparticles. RSC Adv. **5**, 84782–84789 (2015)

17. M. Suzuki, S.I. Fullem, I.S. Suzuki, L. Wang, C.J. Zhong, Observation of superspin-glass behavior in Fe_3O_4 nanoparticles. Phys. Rev. B **79**(2), 024418 (2009)

18. G.S. Parkinson, U. Diebold, J. Tang, L. Malkinski, in *Tailoring the Interface Properties of Magnetite for Spintronics*, ed. by L. Malkinski. ISBN: 978-953-51-0637-1, (2012). doi:10.5772/39101. Available from http://www.intechopen.com/books/advanced-magnetic-materials/tailoring-the-interfaceproperties-of-magnetite-for-spintronics

19. S. Kayal, R.V. Ramanujan, Doxorubicin loaded PVA coated iron oxide nanoparticles for targeted drug delivery. Mater. Sci. Eng. C **30**, 484–490 (2010)

20. S. Laurent, D. Forge, M. Port, A. Roch, C. Robic, E.L. Vander, R.N. Muller, Magnetic iron oxide nanoparticles: synthesis, stabilization, vectorization, physicochemical characterizations, and biological applications. Chem. Rev. **108**, 2064–2110 (2008)

21. M. Mahmoudi, S. Sant, B. Wang, S. Laurent, T. Sen, (2011) Superparamagnetic iron oxide nanoparticles (SPIONs): development, surface modification and applications in chemotherapy. Adv. Drug Deliv. Rev. **63**, 24–28

22. H. Zhang, Q. Wang, L. Li, Dehydration o f water-plasticized (polyvinyl alcohol) systems: particular behavior of isothermal mass transfer. Polym. Int. **58**, 97–104 (2009)

23. M.S. Nasari, F. Davar, T. Mahmoudi, A simple route to synthesize nanocrystalline nickel ferrite ($NiFe_2O_4$) in the presence of octanoic acid as a surfactant. Polyhedron **28**, 1455–1458 (2009)

24. L. Ghazanfari, M.E. Khosroshahi, Effects of coating and stirring on superparamagnetic iron oxide nanoparticles size and magnetic characteristics. Int. J. Innov. Res. Sci. Eng. Technol. **4**, 6659–6666 (2015)

25. W.B. White, B.A. DeAngelis, Interpretation of the vibrational spectra of spinels. Spectrochem. Acta **23A**, 985–995 (1967)

26. T. Shimada, T. Tachibana, T. Nakagawa, T.A. Yamamoto, Site occupation study of $ZnFe_2O_4$ and $NiFe_2O_4$ by far-infrared reflectivity. J. Alloy. Compd. **379**, 122–126 (2004)

27. S. Yan, J. Geng, J. Chen, L. Yin, Y. Zhou, E. Zhou, Preparation of $Ni_{0.65}Zn_{0.35}Cu_{0.1}Fe_{1.9}O_4/SiO_2$ nanocomposites by sol–gel method. J. Cryst. Growth **262**, 415–419 (2004)

28. Z.M. Tian, S.L. Yuan, S.Y. Yin, L. Liu, J.H. He, H.N. Duan, P. Li, C.H. Wang, Exchange bias effect in a granular system of $NiFe_2O_4$ nanoparticles embedded in an antiferromagnetic NiO matrix. Appl. Phys. Lett. **93**, 222505 (2008)

29. S.S. Starchikov, I.S. Lyubutin, C.R. Lin, Y.T. Tseng, K.O. Funtov, Y.L. Ogarkova, T.V. Dmitrieva, A.G. Ivanova, Synthesis and magnetic properties of the chromium-doped iron sulfide $Fe_{1-x}Cr_xS$ single crystalline nanoplates with a NiAs crystal structure. Phys. Chem. Chem. Phys. **17**, 15829–15836 (2015)

30. V.M. Gaikwad, S.A. Acharya, Investigation on magnetic behaviour of $BiFeO_3$: SPIN glass view point. Adv. Mat. Lett. **5**(3), 157–160 (2014)

31. D. Peddis, C. Cannas, G. Piccaluga, E. Agostinelli, D. Fiorani, Spin-glass-like freezing and enhanced magnetization in ultra-small $CoFe_2O_4$ nanoparticles. Nanotechnology **21**(12), 125705 (2010)

32. H. Wang, T. Zhu, K. Zhao, W.N. Wang, C.S. Wang, Y.J. Wang, W.S. Zhan, Surface spin glass and exchange bias in Fe_3O_4 nanoparticles compacted under high pressure. Phys. Rev. B **70**, 092409 (2004)

33. H.T. Yang, D. Hasegawa, M. Takahashi, T. Ogawa, Achieving a noninteracting magnetic nanoparticle system through direct control of interparticle spacing. Appl. Phys. Lett. **94**, 013103 (2009)

34. G. Catalan, J.F. Scott, Physics and applications of bismuth ferrite. Adv. Mater. **21**, 2463–2485 (2009)

35. SAT Redfern, C. Wang, J.W. Hong, G. Catalon, J.F. Scott, Elastic and electrical anomalies at low-temperature phase transitions in $BiFeO_3$. J. Phys. **20**, 452205 (2008)

36. S. Rana, R.S.M. Srivastava, M. Sorensson, R.D.K. Misra, Synthesis and characterization of nanoparticles with magnetic core and photocatalytic shell: anatase TiO_2:$NiFe_2O_4$ system. Mater. Sci. Eng. B **119**, 144–151 (2005)

37. R.D.K. Misra, S. Gubbala, A. Kale, W.F. Egelhoff Jr., A comparison of the magnetic characteristics of nanocrystalline nickel, zinc, and manganese ferrites synthesized by reverse micelle technique. Mater. Sci. Eng. B **111**, 164–174 (2004)

38. A.H. Morrish, K.H. Haneda, Magnetic structure of small $NiFe_2O_4$ particles. J. Appl. Phys. **52**, 2496–2498 (1981)

39. S. Chikazumi, *Physics of Magnetism*. (Wiley, New York, 1959)

40. M. George, A.M. John, S.S. Nair, P.A. Joy, M.R. Anantharaman, Finite size effects on the structural and magnetic properties of sol–gel synthesized $NiFe_2O_4$ powders. J. Magn. Magn. Mater. **302**, 190–195 (2006)

41. M.A. Gabal, Y.M.A. Angari, M.W. Kadi, Structural and magnetic properties of nanocrystalline $Ni_{1-x}Cu_xFe_2O_4$ prepared through oxalates precursors. Polyhedron **30**, 1185–1190 (2011)

42. E.C. Stoner, E.P. Wohlfarth, A mechanism of magnetic hysteresis in heterogeneous alloys. Philos. Trans. R. Soc. Lond. A **240**, 599–642 (1948)

43. C. Tannous, J. Gieraltowski, The Stoner–Wohlfarth model of ferromagnetism. Eur. J. Phys. **29**, 475–487 (2008)

44. K.A. Shaykhutdinov, S.V. Semenov, D.A. Balaev, M.I. Petrov, N.V. Volkov, Hysteresis of magnetoresistance in granular $La_{0.7}Ca_{0.3}MnO_3$ at low temperatures. Phys. Solid State **51**, 778–780 (2009)

45. K.A. Shaykhutdinov, S.I. Popkov, S.V. Semenov, D.A. Balaev, A.A. Dubrovskiy, K.A. Sablina, N.V. Sapronova, N.V. Volkov, Low-temperature resistance and magnetoresistance hysteresis in polycrystalline $(La_{0.5}Eu_{0.5})_{0.7}Pb_{0.3}MnO_3$. J. Appl. Phys. **109**, 053711 (2011)

46. E. DeBiasi, R.D. Zysler, C.A. Ramos, H. Romero, D. Fiorani, Surface anisotropy and surface-core interaction in Co–Ni–B and Fe–Ni–B dispersed amorphous Nanoparticles. Phys. Rev. B **71**, 104408 (2005)

47. E. DeBiasi, C.A. Ramos, R.D. Zysler, H. Romero, Large surface magnetic contribution in amorphous ferromagnetic nanoparticles. Phys. Rev. B **65**, 144416 (2002)